SAND REPORT
SAND2005-1080
Unlimited Release
Printed February 2005

Investigation of the Effects of Intense Pulsed Particle Beams on the Durability of Metal-to-Plastic Interfaces

Timothy J. Renk, Paula P. Provencio, S. V. Prasad, T. E. Buchheit, V. Engelko, D. McNulty, T. D. Petersen, and D. W. Petersen

Prepared by
Sandia National Laboratories
Albuquerque, New Mexico 87185 and Livermore, California 94550

Sandia is a multiprogram laboratory operated by Sandia Corporation,
a Lockheed Martin Company, for the United States Department of Energy's
National Nuclear Security Administration under Contract DE-AC04-94-AL85000.

Issued by Sandia National Laboratories, operated for the United States Department of Energy by Sandia Corporation.

Available to DOE and DOE contractors from
U.S. Department of Energy
Office of Scientific and Technical Information
P.O. Box 62
Oak Ridge, TN 37831

Telephone: (865)576-8401
Facsimile: (865)576-5728
E-Mail: reports@adonis.osti.gov
Online ordering: http://www.doe.gov/bridge

Available to the public from
U.S. Department of Commerce
National Technical Information Service
5285 Port Royal Rd
Springfield, VA 22161

Telephone: (800)553-6847
Facsimile: (703)605-6900
E-Mail: orders@ntis.fedworld.gov
Online order: http://www.ntis.gov/help/ordermethods.asp?loc=7-4-0#online

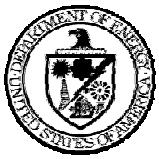

SAND2005-1080
Unlimited Release
Printed February 2005

Investigation of the Effects of Intense Pulsed Particle Beams on the Durability of Metal-to-Plastic Interfaces

Timothy J. Renk
Beam Applications and Initiatives Department

Paula P. Provencio
Radiation-Solid Interactions Department

Somuri V. Prasad and Thomas E. Buchheit
Microsystems Materials and Mechanical Behavior Department

Sandia National Laboratories
P. O. Box 5800
Albuquerque, NM 87185-1182

Vladimir Engelko
D. V. Efremov Scientific Research Institute of the Electrophysical Apparatus
St. Petersburg, Russia

Donald E. McNulty
DePuy Orthopaedic, Inc., Warsaw, IN

Thomas D. Petersen
University of California (San Diego)

Donald W. Petersen
University of Alabama (Birmingham)

Abstract

We have investigated the potential for intense particle beam surface modification to improve the mechanical properties of materials commonly used in the human body for contact surfaces in, for example, hip and knee implants. The materials studied include Ultra-High Molecular Weight Polyethylene (UHMWPE), Ti-6Al-4Al (titanium alloy), and Co-Cr-Mo alloy. Samples in flat form were exposed to both ion and electron beams (UHMWPE), and to ion beam treatment (metals). Post-analysis indicated a degradation in bulk properties of the UHMWPE, except in the case of the lightest ion fluence tested. A surface-alloyed Hf/Ti layer on the Ti-6Al-4V is found to improve surface wear durability, and have favorable biocompatibility. A promising nanolaminate ceramic coating is applied to the Co-Cr-Mo to improve surface hardness.

Table of Contents

Investigation of the Effects of Intense Pulsed Particle Beams on the Durability of Metal-to-Plastic Interfaces

I. INTRODUCTION

There are a number of mechanical applications where materials are used in sliding or other kinds of mechanical contact. For example, cobalt-chromium-molybdenum (Co-Cr-Mo) alloy and Ultra-High Molecular Weight Polyethylene (UHMWPE) form a flat sliding joint in artificial knee implants. In such cases, it is desirable to limit the wear generated by the action of the sliding motion, and mechanical contact motion in general. Other issues like debris particle (size, shape and morphology) interactions with the body, friction, etc., play a more important role in biocompatibility. In other words, sliding interactions result in debris generation—and the interaction of wear debris with the human body is a crucial factor in determining the biocompatibility of the material system. While the materials addressed in this report are specifically for in-body applications, the lessons learned here have potential applicability to a larger body of materials of interest to the DOE complex.

We focus here on three materials that are used in replacement hip and knee hardware implanted in the human body: the UHMWPE mentioned above, titanium alloy (Ti-6Al-4V), and Co-Cr-Mo alloy. Ti-6Al-4V is a common Ti alloy, used in many applications, whose bulk and surface mechanical properties have been extensively studied and are well known. It is used in the body even though the alloying elements, aluminum and vanadium, are toxic to the body. This is due to its extensive database of known properties. The predominant in-body use of Ti-6Al-4V is for interfacing with bone, and thus bone on-growth is encouraged, as opposed to mechanical motion. It is well suited for this, evidently because its high elastic modulus encourages the formation of bone and bone on-growth. The same elastic properties in the bulk, however, lead to poor surface mechanical properties, i.e. the Ti surface is relatively soft, and wears readily in contact with other materials.

Co-Cr-Mo, in contrast, is a significantly harder metal alloy, and has become the favored metal to use in the body for mechanical sliding contacts. For instance, the ball in a hip implant is typically made of Co-Cr-Mo. The ball (leg side) contacts and is surrounded by a cup made of UHMWPE, which is locked into a spherical shell made of Ti-6Al-4V. The shell is then in turn press-fit into the hip socket (acetabulum). The contact surface is then between the Co-Cr-Mo and the UHMWPE.

At present, typical lifetimes of these materials in the body are 10 - 20 years. While well-designed implants in older patients often have 95% success rates at 10-year follow-up, the survivorship after 10 years typically deteriorates.[1,2] Younger patients who require joint replacement typically have much higher failure rates.[3-5] The primary reason for this is excessive wear on contact surfaces, in particular the Co-Cr-Mo and UHMWPE surfaces.[6,7] The UHMWPE wears and sheds a considerable amount of fine particles, either caused by the direct contact, or because of third-body particles that get trapped between the two primary surfaces. The wear particles migrate away from the interface point, and give rise to inflammatory responses from the body. The particles also cause bone remission between the Ti alloy and the bone which has grown into it, leading to loosening of the press-fit leg shaft (femur), as well as possibly wear-through of the UHMWPE cup. It is often the case that the original 6 mm PE cup thickness is worn completely through.

It might be expected that replacing the PE with Co-Cr-Mo would lead to a lessened wear and debris particle generation rate. This resulting metal-to-metal contact would indeed lead to a smaller wear debris volume. But the wear part-

cles themselves would be finer, and they would of course be metal instead of plastic. The body reacts more adversely to finer wear particles, and there are long-term health and toxicity issues connected with circulating metal particles in the body.

Another possible materials choice for such a wear surface is ceramic. Such ceramic balls and cups are widely used in Europe, which has resulted in significantly lower wear rates. But bulk ceramic is of course brittle, and fractures caused by, for example, sudden stresses such as a fall are potentially catastrophic. In addition to the trauma of the fracture itself, unless all of the ceramic particles are removed from such a fracture, the residual particles, which can be expected to be quite fine, can wreak havoc on plastic or metal replacement hardware.

The general goal of this investigation is then to improve the wear durability of the materials discussed above. The measure of this improvement is post-modification performance gain as indicated by wear testing of flat samples, not in-body trials of actual modified replacement parts. Successful incorporation of modified materials into real-world hardware is the subject of future work.

To summarize the discussion above, the materials to be investigated for this report are listed here, with the main modification issues for each:

1) UHMWPE: Surface hardening to improve wear durability. The goal is to use ion and electron beam treatment to produce cross-linking of the plastic, leading to a tougher and more wear-resistant surface.
2) Ti-6Al-4V: Surface alloying to reduce wear. Results of such wear improvement have been previously reported.[8] Here, we will investigate the modification of the near-surface region to a) add a biocompatible material, and b) to passivate the toxic Al and V alloying elements.
3) Co-Cr-Mo: Coating of the surface with a modified ceramic, to reduce surface wear.

Figure I. Photograph of RHEPP-1 treatment vacuum tank. For thin-film deposition, the table shown is removed and ablation target substituted in its place.

The substrate materials have been supplied as follows: UHMWPE from DePuy Orthopedics, consisting of Marathon™ Co-60 radiation-crosslinked and annealed PE; and Ti-6Al-4V and Co-Cr-Mo from Alvarado Orthopedic. Application of the coating and coating treatment were undertaken at Sandia National Laboratories (SNL) in Albuquerque. Some of the PE was treated with electron beams at Efremov Institute in St. Petersburg, Russia, with funds supplied by this LDRD project. Post-analyses of both ion- and electron beam-treated materials were done either at SNL, or at DePuy and/or Alvarado Orthopedic. In the latter case, analysis costs were borne by the respective facilities.

The ion and electron beam treatment facilities and setup are discussed in Section II. Details of the treatment and effects of the three materials are given in Sections IIIa-c.

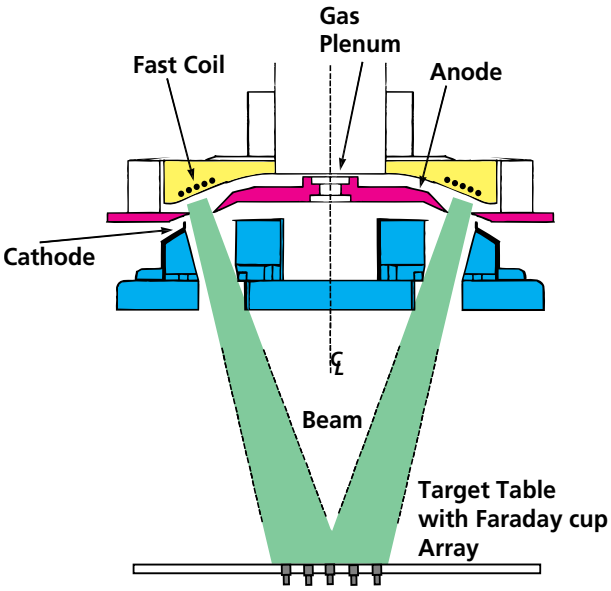

Figure 2. Schematic side view of Diode geometry including MAP and treatment area.

II. EXPERIMENTAL FACILITIES AND TREATMENT SETUP

a. Ion beam treatment – RHEPP-1 (SNL)

The RHEPP-1 facility has been described elsewhere.[8-10] A photograph of the RHEPP-1 treatment tank is shown in Fig. 1. The annular ion beam exits the cathode slot, shown at top, and propagates downward towards the circular trays on which samples for treatment are normally located. The treatment geometry for surface modification experiments is schematically depicted in Fig. 2. The ion beam achieves a weak focus at about 40 cm from the ion diode. Treatment fluence can be adjusted by varying the sample distance from the beam centerline. An array of Faraday cups measures the beam fluence in the vicinity of treated samples. In the case of the UHMWPE treatment (Section IIIa below), the beam was partially blocked just beyond the generation point by installing sheet metal wedges periodically spaced in azimuth. This allows for beam attenuation while still preserving reasonable azimuthal symmetry at the sample location.

Beam voltage varied between 500 and 850 kV, but was typically in the 750-800 kV range for the treatment detailed below. From TRIM[11] calculations, the penetration range for ions of this voltage is approximately 1 μm. Current densities on target ranged from 5-10 A/cm^2 in the case of the attenuated beam, to over 200 A/cm^2 for ablating the ceramic targets (Section IIIc). Ion species will be discussed in the Sections below.

b. Electron beam treatment – GESA I and II, Efremov Scientific Research Institute of Electrophysical Apparatus, St. Petersburg, Russia.

Electron beams can also be used for surface modification, but since the penetration of electrons is much deeper than for ions, either the generation voltage must be reduced (by the square root of the mass ratio), or the pulse duration must be increased in proportion to achieve a specific energy deposition (J/g) similar to ions. At Efremov Institute, the capability of generating electron beams in the 100 – 400 keV range, with long pulse durations (up to 500 μsec) has been developed.[12,13] This has been done through careful cathode source design, including multi-point emitters of carbon fiber bundles with series resistors to limit the cathode plasma velocity and hence gap closure speed. Emission from secondary surfaces is controlled, and the diode voltage held relatively constant throughout the power pulse. The electrons are directed to the treatment area by solenoidal guide fields.

The effect of electron treatment on the target material must be carefully modeled. This is because the electron beam is partially reflected from the material surface, and the reflected flux returns to the diode region. This interaction leads to a modification of the remaining portion of the power pulse. The level of reflected power depends upon the target material. While treatment of various materials has been undertaken, predominantly metals, for this Report electrons are used to expose the UHMWPE only. This is detailed in Section IIIa.

III. Modification Experiments

IIIa. Ultra-High-Molecular Weight Polyethylene (UHMWPE)

This as-provided form of PE investigated here is a product of DePuy Orthopaedic (Warsaw, IN). This form of PE is treated with gamma radiation prior to insertion in the body, which has proved to be a factor in its wear durability.[14] The bulk material is treated with whole-body Co-60 radiation to a dose of 5 MRads, and then re-melted at ~ 150°C (melting point about 135°C). The Co-60 radiation induces cross-linking, and the re-melting acts to remove the free radicals which are produced by the x-ray irradiation. If the free radicals are not removed, the PE is observed to suffer mechanical deterioration and subsequent excessive wear if used in in-body implants.[15-17] The resulting product is named Marathon™.

The level of Co-60 irradiation has been studied by various researchers, and levels as high as 100 MRads have been used. However, such high doses have lead to a decrease in mechanical performance, as the bulk material becomes brittle. We investigate here the possibility that additional cross-linking may be produced in the near-surface region of the UHMWPE, without affecting the bulk properties, by pulsed intense surface heating, either by electron or ion beams. The fluence level must be carefully chosen, however, since the melting point of UHMWPE (~ 135°C) is far lower than the metals or ceramics that are typically subjected to such thermal processing.

In the case of the electron beam treatment at Efremov, simulations were performed of the PE response to electron exposure, as a function of electron energy, current density, and pulse width. Examples of two such simulations are shown in Fig. 3a and 3b. The voltage in these cases is a constant over the pulse duration. Note that the second electron pulse produces a deeper heating profile, while the surface temperature excursion is still limited to 130°C maximum. This is due to the greater penetrating power of the 400 keV electrons in the second case. Simulated responses for other voltage shapes, such as triangular, were also done,

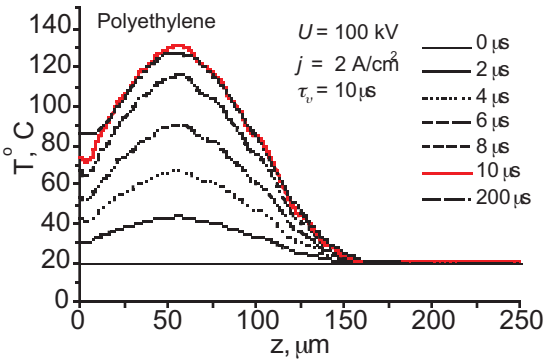

Figure 3a. Simulation, response of UHMWPE to 100 kV electron beam from GESA-1. Y-axis is in degrees C.

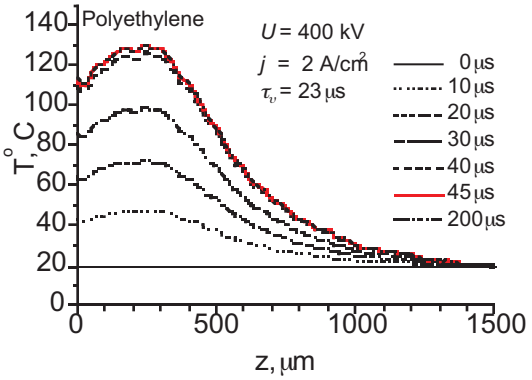

Figure 3b. Simulation, response of UHMWPE to 400 kV electron beam from GESA-11. Y-axis is in degrees C.

and they predict a more peaked temperature profile, but still limited to a similar surface maximum temperature as described above.

Samples of bulk Marathon UHMWPE were machined into ASTM 'dogbones'. i.e. tensile bars -rectangular flats with a narrowed-segment in the middle. Sets of 4 samples each were subjected to two treatment protocols at Efremov, on the GESA-1 and GESA-2 electron beam facilities. The samples were exposed on a) one side only, and b) both sides.

For GESA-I treatment, initial test conditions investigated were: pulse durations of 20 μsec at 120 kV, current density 1 – 7 A/cm^2, and pulse number of 1, 10, 25, and 50. In all cases, a color change was observed, from translucent white to a yellowish tone. This implies a considerable amount of cross-linking and free radical formation. The 50 pulse treatment lead to surface exfoliation, and measurements indicated that the microhardness of the samples decreased for the 25 and 50-pulse samples. The final treatment protocol was selected to be 10 pulses.

For GESA-II treatment, an initial treatment level of : current density 2 A/cm^2, voltage of 300 kV, and pulsewidth 37 μsec – was chosen, consistent with modeling predictions. This produced a surface disruption in the PE, so a reduced pulsewidth of 20 μsec was chosen. Even at this reduced fluence, surface disruption occurred with 10 treatment pulses, so a treatment level of 2 pulses was used for the test samples. The yellowish tone again appeared in the treated surfaces, with also the appearance of point defects inside the treated layer.

In the case of ion exposure on RHEPP-1, it was not clear what the appropriate level of treatment should be, since the surface temperature excursion was expected to exceed 140° C in all cases, due to the short ion range (about 3 μm at most). For the first treatment attempt, the treatment gas injected into MAP was chosen to be Ar, which yields a mixed carbon-argon beam. In the past, this type of beam has produced less surface roughening than surfaces exposed to either hydrogen or nitrogen. Mechanical beam blocks were inserted into the diode region just downstream of the A-K gap, blocking out an estimated 70% of the normal ion beam. An initial test exposure was conducted of three dogbones at three different fluences, the highest at over 1 J/cm^2. The two lower fluences were chosen for the full set treatment protocols. In both cases, the center of the kneckdown was subjected to 25 ion pulses. The lower fluence was about 0.3 – 0.4 J/cm^2, with the higher level at 0.65 J/cm^2, and with an estimated ± 40% scatter in the fluence magnitude over the 25 pulses. This is well below the typical fluence levels used in metals treatment.

Surface profilometry measurements of surface were made after RHEPP treatment with a 1-D Dektak. Scans were made of the untreated area, and extending across the treatment interface. The lower level of treatment produced a slight increase in surface roughness (R_a in-

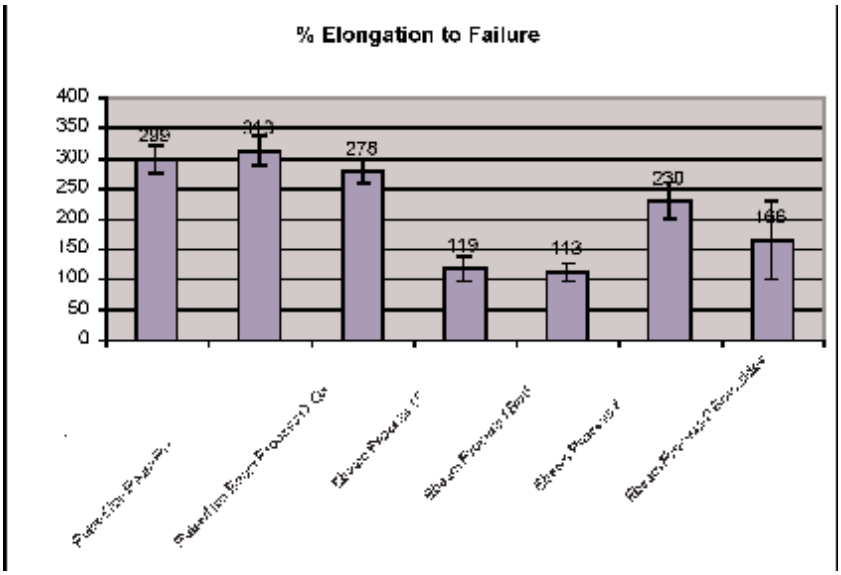

Figure 4a. Elongation to failure data, for control, ion beam treated (Ne beam, low fluence, 10 pulses) - next 2, and electron beam treated (last 4 bars).

creased from 2.1 μm to 2.4 μm), but the higher treatment level removed 25 μm of material from the dogbone area. This is clearly an overtreatment of the PE.

The PE treated by electron beams, and this first round of ion-treated PE, was then delivered to DePuy and analyzed for changes in bulk properties. The result was rather surprising. All samples suffered declines in % elongation to failure, the ion-treated samples by about 15%, the electron-treated samples by as much as 60%. All samples showed about a 50% decline in ultimate strength. Yield strength and Young's modulus appeared roughly unaffected. This serious decline in bulk mechanical performance was totally unexpected, since both electron and ion beam treatment have been assumed to be surface treatments, without the ability to produce changes in bulk properties. These test results prove otherwise.

We elected to try a second round of ion treatment, at both a lower fluence, and reduced number of pulses, since the Russian work had shown that a pulse number of 2 to 10 produced better hardness results for electron treatment. The gas injection was switched from Ar to Ne, which gives a beam of less carbon amount, and again operated with mechanical beam blocks. Two sample sets were treated, at an estimated fluence of 0.1 and 0.2 J/cm^2 ('low' and 'high'), respectively, with again about a 40-50% scatter in this number, with ten pulses in each case, and single-sided only. Note that both the fluences and pulse numbers are lower than for the first round.

This time, the bulk testing by DePuy produced more favorable results. Data are shown in Figs 4a and 4b for both %elongation to failure, and for ultimate strength. In both Figures, the left-most bar is the control (untreated Marathon), the next two bars are for 'low' and 'high' fluence ion Ne ion exposures, and the next four bars are for the two electron beam exposure protocols, single and double-sided. Note that the data for the Russian e-beam exposures are very similar, and show a significant decline in the two bulk properties, as stated above. Both Ne beam exposure sets show values very close to the control values, although the ultimate strength has apparently decreased by 10-15%.

Based upon these results, it was decided to prepare and expose a set of samples for Pin-on-

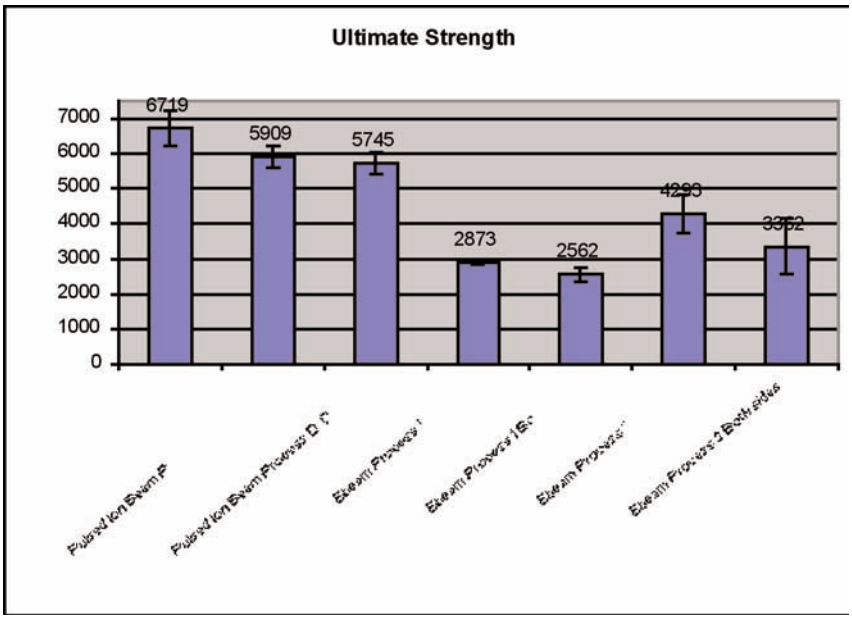

Figure 4b. Ultimate strength data, for control, ion beam treated (Ne beam, low fluence, 10 pulses) - next 2, and electron beam treated (last 4 bars).

Disk wear testing. Sets of disks were exposed to 'low' and 'high' Ne fluence, and now await wear testing, the result of which will be included in a future publication.

IIIb. Surface alloying of Ti-6Al-4V

We have previously reported[8,18] on the addition of a Hf-rich surface layer to the near-surface region of Ti-6Al-4V alloy by ion beam surface alloying. A 1 micron-thick layer of 50at% Hf –50at% Ti was deposited on the alloy surface by dual magnetron sputtering. [This was previously reported, incorrectly, as a 20at% Hf – 80at% Ti layer.] This surface was then exposed to 35 pulses of the MAP nitrogen beam, in a range of fluences, from less than 1 J/cm^2 to 3 J/cm^2. Portions of the treated surface were then subjected to a linear wear cycle of a reciprocating tribometer over 1000 cycles. The counterface was a Si_3N_4 ball with 10 gms applied force, operating in a dry nitrogen atmosphere.

Figs. 5a-c show the measured friction coefficients for the following three cases: a) Hf-rich coating treated at < 1 J/cm^2 fluence, b) coating treated at 3 J/cm^2 fluence (maximum), and c) for comparison, a Ti-6Al-4V surface wthout the Hf-rich coating that has been ion beam-treated with a fluence of 1 – 1.5 J/cm^2. In all case, the vertical axis indicates the friction coefficient, and the horizontal axis the number of cycles. A friction coefficient of 0.6 or above generally indicates a surface worn by the counterface, with attendant wear debris and prominent wear track. Note that cases a) and c) show such a relatively high friction coefficient, but the behavior is much different in case b). In the latter case, the friction coefficient remains very low, never rising about 0.25, for the entire 1000 cycles. As the comparison between a) and c) shows, beam treatment of the uncoated Ti-6Al-4V does not lead to the improvement seen in case b). Thus the improvement in friction coefficient is clearly due to the addition of the Hf-rich coating, and to the beam treatment of this coating to the level of 3 J/cm^2.

After the tribological testing, SEM images were taken of the wear tracks associated with the various locations. Examples of two of the tracks

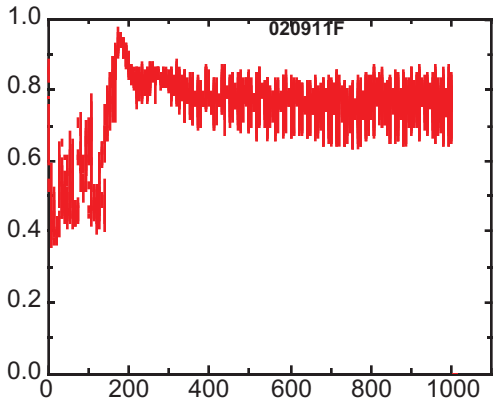

Figure 5a. Friction coefficient, Hf/Ti coating, treated with < 1 J/cm^2.

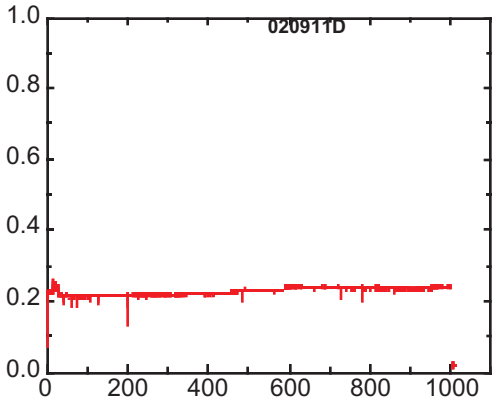

Figure 5b. Friction coefficient, Hf/Ti coating, treated with 3 J/cm^2.

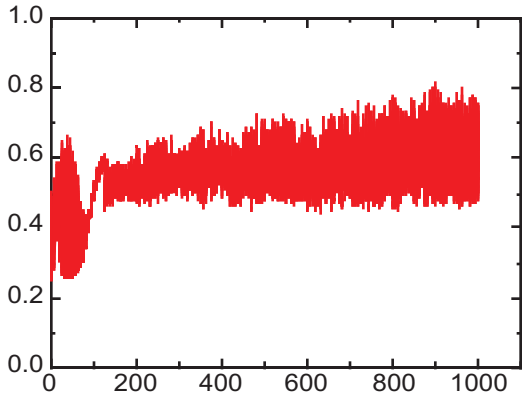

Figure 5c. Friction coefficient, uncoated Ti-6-4 treated with 1 - 1.5 J/cm^2.

are shown in Figs. 6a (1 J/cm^2) and 6b (3 J/cm^2). The friction coefficient in the 1 J/cm^2 case showed similar behavior to the 3 J/cm^2, case, except that there were a few cycles of high coefficient in the very beginning of the test cycle. The wear scar in Fig 6a, while significantly less prominent than the coated but untreated case (not shown), is much worse than for Fig 6b (3 J/cm^2). In the latter, the wear scar has virtually disappeared, and in fact the dark material shown in the (false-color) image is probably from the Si_3N_4 counterface. Given that Si_3N_4 is three times harder than as-manufactured Ti-6Al-4V, this is evidence of a very significant reduction in wear of the surface alloyed Hf-Ti.

In addition to the SEM imaging, sections of near-surface material were removed from the treated Hf-Ti surface by Focused Ion Beam (FIB) milling, then examined by cross-sectional transmission electron microscopy (XTEM). FIB cuts were studied from the treated areas at 1, 2.25, and 3 J/cm^2, and shown in Figs 7a-c, respectively. (Note the direction of the sample surface in each image).

In all three Figures, the coating microstructure is evident, i.e. a columnar structure typical of films deposited by unbalanced magnetron sputtering. In Fig 7a, the layer shows the least modification. [Surface is at lower left.] There is a zone behind the original 1 μm coating thickness, totaling 0.1μm, in which Hf has diffused during the melt phase. This is consistent with the modeling prediction for this treatment fluence, which is for a melt depth of 1.1 μm total. The friction coefficient behavior already shows a significant change from the coated but untreated layer at this fluence, even for this case of only slight evident change in the coated layer.

For the 2.25 J/cm^2 fluence case (Fig7b), there is more layer modification evident. [Surface is at lower left.] The original thickness has been reduced by about 0.2 μm by surface ablation due to the ion beam. But a zone of modified structure appears behind the coating, through which substantial Hf has diffused during the melt phase. The diffusion zone appears as a chaotic-looking region behind the original coating, with a width of about

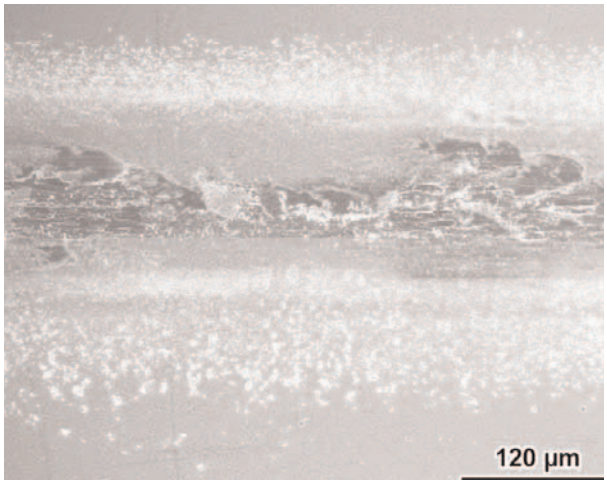

Figure 6a. Wear track, coated Hf/Ti treated with 1 J/cm^2.

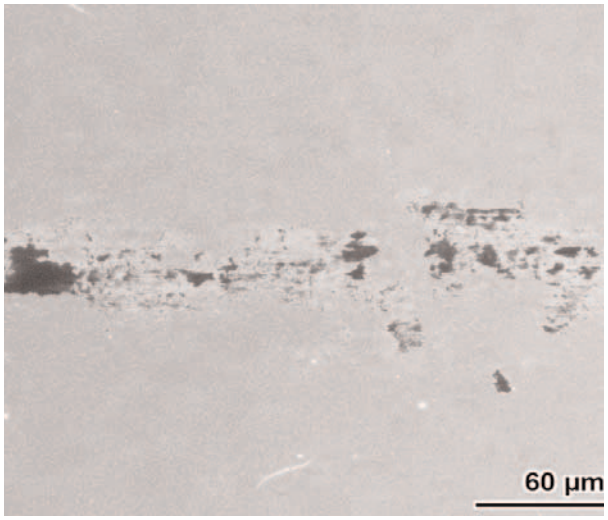

Figure 6b. Wear track, coated Hf/Ti treated with 3 J/cm^2.

0.6 μm. In addition, the surface has been roughened, from R_a = 28 nm to 74 nm after beam treatment. Model predictions for this fluence are: melt thickness of 1.75 μm, and melt duration of about 1 μsec. The ablated zone varies along the surface, but an average of 0.2 μm is removed. This is an average of 6 nm removed per ion pulse. However, we can roughly estimate the diffusion length per pulse by considering RT (4Dt) scaling, where D is a typical diffusion coefficient. Setting t ~ 1μsec and D ~ 5e-4 cm^2/sec, which is a reasonable estimate for the diffusion for Hf in Ti, we obtain ~ 0.5 μm for the diffusion length per pulse. Thus liquid-phase diffusion of Hf into the Ti substrate can easily exceed the removal rate of the Hf from the surface by the action of the ion beam.

At 3 J/cm^2 (Fig. 7c), up to 0.4 μm of the original coating has been removed by ablation (11 nm per pulse), and the diffusion layer behind the coating now extends to a thickness that is equal to or greater than the amount of the remaining original coating thickness. [Surface is at lower right.] The remnant of the original coating and the diffusion layer together appear as a dark zone in the lower right part of the image. Behind this zone, there is another 1.5 μm distance in which substantial microstructure change has taken place. Hf has also diffused into this zone, but at a lower concentration. Model predictions for this fluence are : melt depth 2.45 μm, and melt duration 1.9 μsec. Surface roughness has increased to R_a ~ 150 nm.

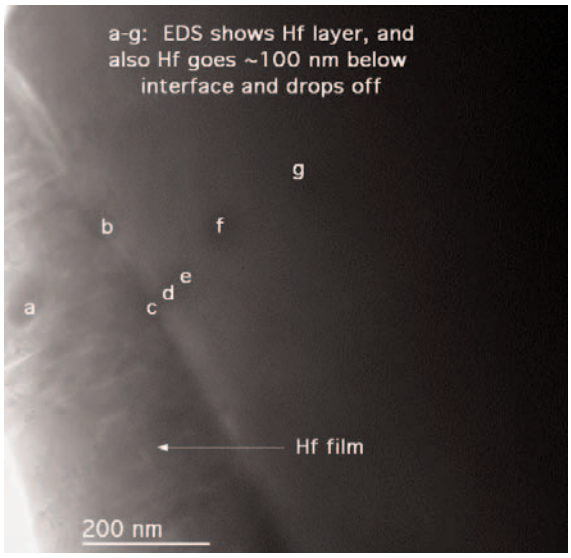

Figure 7a. XTEM cross-sectional view of Hf/Ti layer, 35 pulses at 1 J/cm^2. Surface is at lower left.

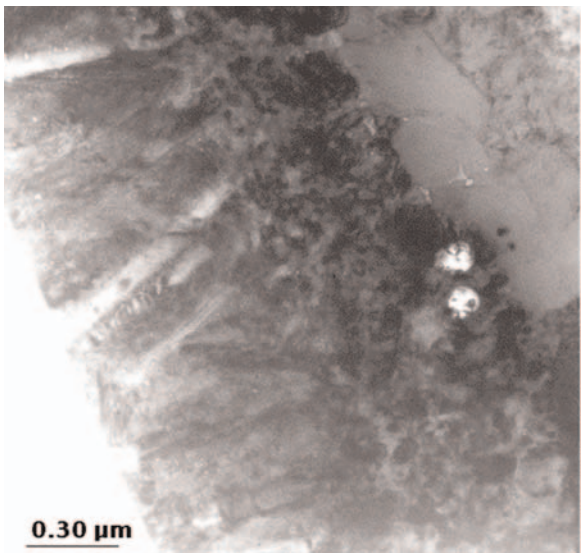

Figure 7b. XTEM cross-sectional view of Hf/Ti layer, 35 pulses at 2.25 J/cm^2. Surface is at lower left.

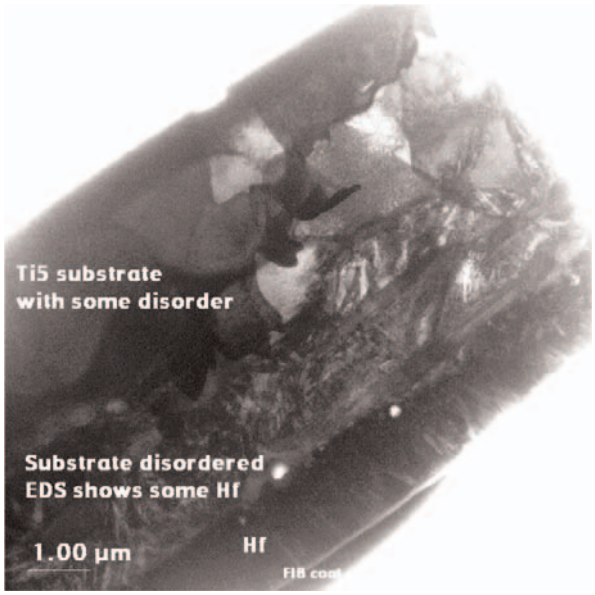

Figure 7c. XTEM cross-sectional view of Hf/Ti layer, 35 pulses at 3 J/cm^2. Surface is at lower right.

The depth of the microstructure change seen in Fig. 7c is not constant, but varies across the treated zone for the 3 J/cm^2 sample. Lower magnification images of the two higher-fluence treatments can be seen in Figs. 8a (2.25 J/cm^2) and 8b (3 J/cm^2). There is some change in the underlying substrate below the coating and diffusion zone in Fig. 8a. But the change is much more substantial in Fig. 8b. A significant conversion to martensitic structure has taken place. This is visible as a network of diagonal 'needle' features. Traces of this conversion appear as far as 6 μm below the surface. This 'deep-lying' zone is well below the heat-affected near-surface region.

Selective Area Diffraction (SAD) was also employed to study grain refinement in the treated samples. The result is shown in Figs. 9a-c (right). Both Figs. 9a and 9b show a polycrystalline grain structure. But the microstructure has clearly changed in Fig. 9c (3 J/cm^2). The grain structure now appears nanocrystalline. This may be contributing to the improved wear properties at this fluence.

In all three sets of images, the original coating looks roughly the same, with only the thickness of the modified zone different in appearance. And yet the behavior of the friction coefficient and wear tracks associated with three different fluences is substantially different. At this point, we cannot identify the exact mechanism for the improvement in mechanical wear properties. The grain-refined microstructure may be a factor, although the friction coefficient and wear track data show improvements even when the microstructure is indicated to be polycrystalline. It could be that the deep-lying zone contributes to the improvement, or possibly the way the coating adheres to the interface has been changed.

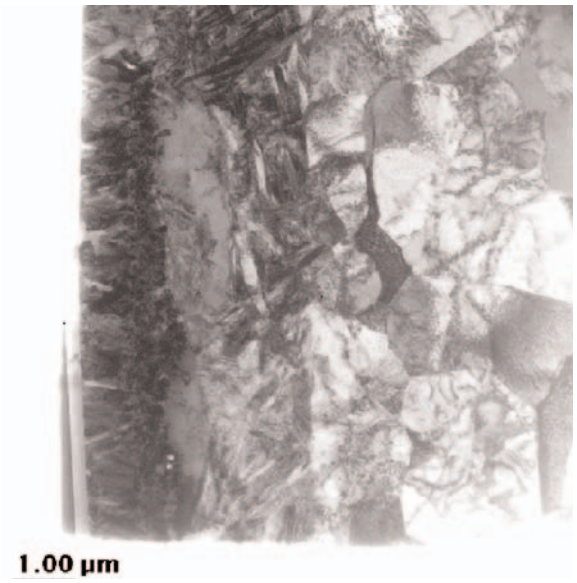

Figure 8a. Low-magnification XTEM cross-sectional view of Hf/Ti layer, 2.25 J/cm^2. Surface is at lower left.

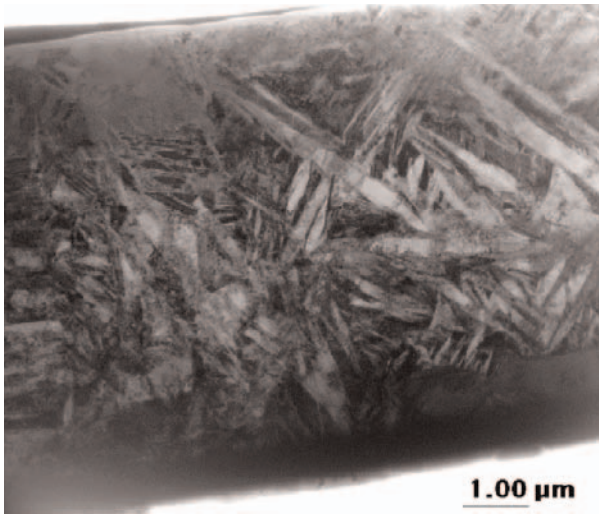

Figure 8b. Low-magnification XTEM cross-sectional view of Hf/Ti layer, 3 J/cm^2. Surface is at bottom.

Biocompatibility testing.

The Hf as a coating component was originally introduced to improve mechanical performance, and was not intended to address biocompatibility gain. A literature search found only one reference for Hf in regards to biocompatibility. In the study by Matsuno H. et. Al,[19] wires composed of Hf as well as Ti, Nb, Ta and Re were inserted into the soft (subcutaneous abdominal region) and hard (femoral bone marrow) tissue of rats, for time periods of 2 and 4 weeks. After this time, Histology (2 and 4 weeks) and elemental map (4 week) tests were done. The conclusion was that all the metals tested, including Hf, have good biocompatibility and osteoconductivity.

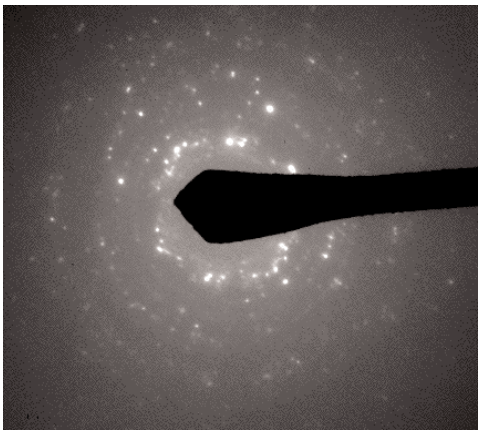

Figure 9a. SAD, Hf/Ti layer, 1.5 J/cm^2

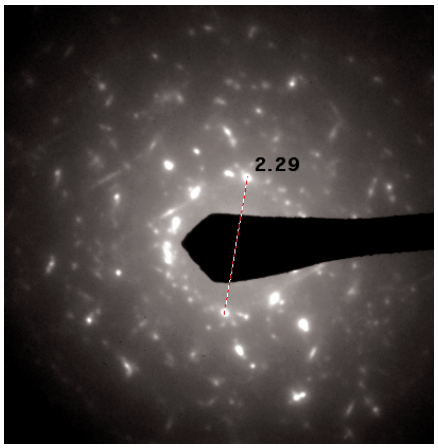

Figure 9b. SAD, Hf/Ti layer, 2.25 J/cm^2

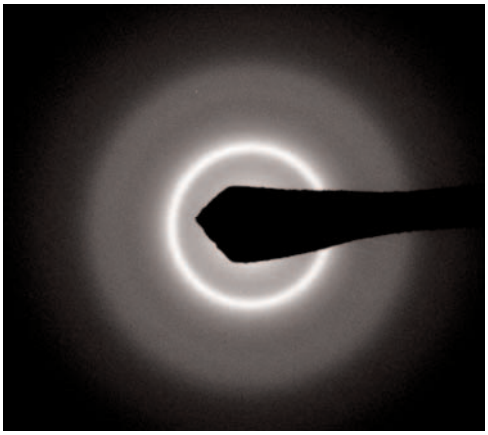

Figure 9c. SAD, Hf/Ti layer, 3 J/cm^2

The best mechanical performance was obtained in this work, as described above, by exposing the Hf-rich coating to 35 ion pulses at 3 J/cm^2. This treatment level was then chosen as the baseline for the bicompatibility and corrosion testing to be described below. The purpose of the corrosion testing was to see if the Hf-modification had any deleterious effects on the corrosion properties of untreated Ti-6Al-4V, which are generally considered to be good.

Cell-culture tests. A set of treated samples was subjected to a procedure known as Hexosaminidase Assay.[20] This is a measure of the propensity of live introduced cells to multiply in the vicinity of a given surface. These cells release the enzyme N-acetyl-B-D-hexosaminidase in proportion to their numbers. It is this enzyme that is measured at the end of a given test period. N-acetyl-B-D-hexosaminidase (hexosaminidase) is a ubiquitous lysosomal enzyme that is thought to be involved in the degradation of glycosylated cellular constituents. It has been demonstrated in many tissues and in different phyla. A p-nitrophenol derivatized substrate can be employed for the spectrophotometric quantification of the activity of hexosaminidase. Its widespread occurrence and its catalytic activity makes hexosaminidase an ideal indicator for analysis of cell numbers.

The cell type chosen for this assay is known as Saos-2. These are osteoblast-like osteosarcoma (cancer) cells, which are harvested for this kind of diagnostic purpose. Three sets of flat disk samples were prepared to receive the cells. These were 1) the Hf-Ti treated disks, 2) as-manufactured Ti-6Al-4V disks, and 3) plastic flats, designated as Control surfaces. All samples were sterilized prior to testing by soaking in 100% reagent alcohol for 1 hour and then rinsed 5x with sterile phosphate buffer saline (PBS). The Saos-2 cells were grown to confluence in 75 cm^2 flasks, and harvested using typsin-EDTA. Cell suspension was then prepared yielding 10^6 cell per ml concentration, and pipetted into 96 well plates to a density of 2 x 10^5 cells per well, along with complete cell culture media (McCoys Media + 10% Fetal Bovine Serum (FBS)). The well plates contained the 0.242

inch diameter flat disks.

Cell activity was studied at Days 3 and 7. At Day 3, media from the wells of the plate containing the samples was aspirated. Wells were rinsed 3x with PBS, and 100 μl of lysate was then placed in the wells with cells and samples and incubated at 37°C for 15 minutes. (Lysate is a detergent which dissolves the cells and thus releases the enzyme, hexosaminidase, from the cell.) Next, 30 μl of lysate from the wells with the sample and cells is then placed in empty well two times (duplicate). Then 30 μl of substrate reagent is placed in the wells with the lysate and incubated for 1 hour. This was followed by 100 μl of "stop" solution that was added to the wells. This reacts and turns the solution yellow in color. Finally, the wells are "read" on a spectrophotometer to yield the optical density measurements that are the experimental results.

The results for the metal disk groups can then be normalized to the Control group (blank or plastic wells). This Assay was repeated at Day 7, the Day 7 cells being fed at Day 3 and Day 5. The results for Days 3 and 7 are summarized in the Tables below, and plotted in Fig. 10.

The Day 3 Results show that Hf/Ti coated samples had a slightly better cell response then the uncoated Ti-6Al-4V samples, but the difference becomes significant at 7 days. The Hf-Ti layer showed a 61% gain in cell activity, compared to the plastic control samples. The as-manufactured Ti-6Al-4V samples showed a 16% gain over the control value. The improved hexosaminidase results for the Hf/Ti coating, especially for Day 7 results, could be due to various factors: 1) improved cellular response to the addition of Hf to the surface chemistry. That is, Hf or Hf-Ti compound may have a positive effect on the cells; or 2) there could be a cellular response to different surface morphology, since the treated and coated samples have different surface morphology than uncoated samples.

Corrosion Tests. Another set of treated Hf/Ti and as-manufactured Ti-6Al-4V samples were subjected to two corrosion measurement procedures. These are called Direct Current Potentiodynamic Polarization Corrosion Testing, and Electrochemical Impedance Spectroscopy. Both corrosion tests were conducted in Hank Balanced Salt Solution (HBSS) at 37C, pH 7.20-7.40 which was de-areated using nitrogen gas (one half hour before starting testing and continuing through the tests).

Cell Culture Results: Hexosaminidase Assay

Day 3 Results	Experiment 1	Experiment 2	**Day 3 Average**	**% of Control**
Control (Blank Well)	1.739 ± 0.150		**1.739 ± 0.150**	**NA**
Uncoated Ti-6Al-4V	1.938 ± 0.084	1.672 ± 0.101	**1.805 ± 0.188**	**104%**
Hf/Ti Coated Ti-6Al-4V	1.936 ± 0.074	1.910 ± 0.055	**1.923 ± 0.018**	**111%**

Day 7 Results	Experiment 1	Experiment 2	**Day 7 Average**	**% of Control**
Control (Blank Well)	1.457 ± 0.440		**1.457 ± 0.440**	**NA**
Uncoated Ti-6Al-4V	2.072 ± 0.720	1.306 ± 0.252	**1.689 ± 0.542**	**116%**
Hf/Ti Coated Ti-6Al-4V	2.241 ± 0.550	2.455 ± 0.489	**2.348 ± 0.151**	**161%**

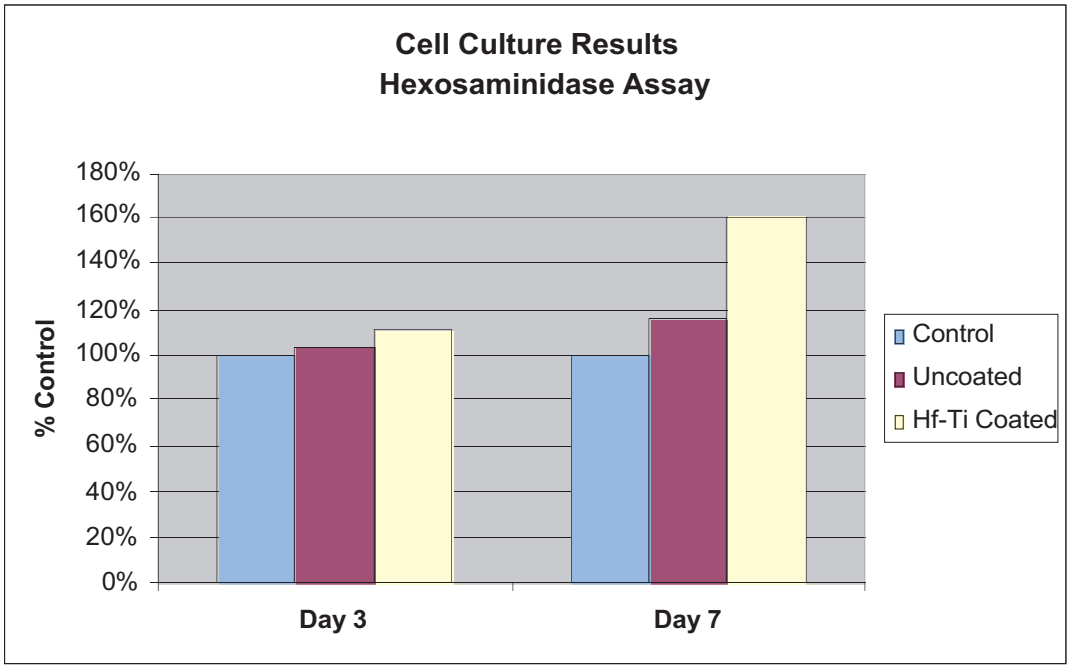

Figure 10. Cell culture performance, 3 and 7 day results.

The results can be summarized in Fig. 11 below. The two voltage-current plots show that the Hf/Ti coated surface exhibits comparable corrosion resistance to the as-manufactured and uncoated Ti-6Al-4V surface. Thus, the coating and beam treatment of the Hf-rich surface layer produced no significant change in the (very good) corrosion resistance of the standard Ti-6Al-4V surface.

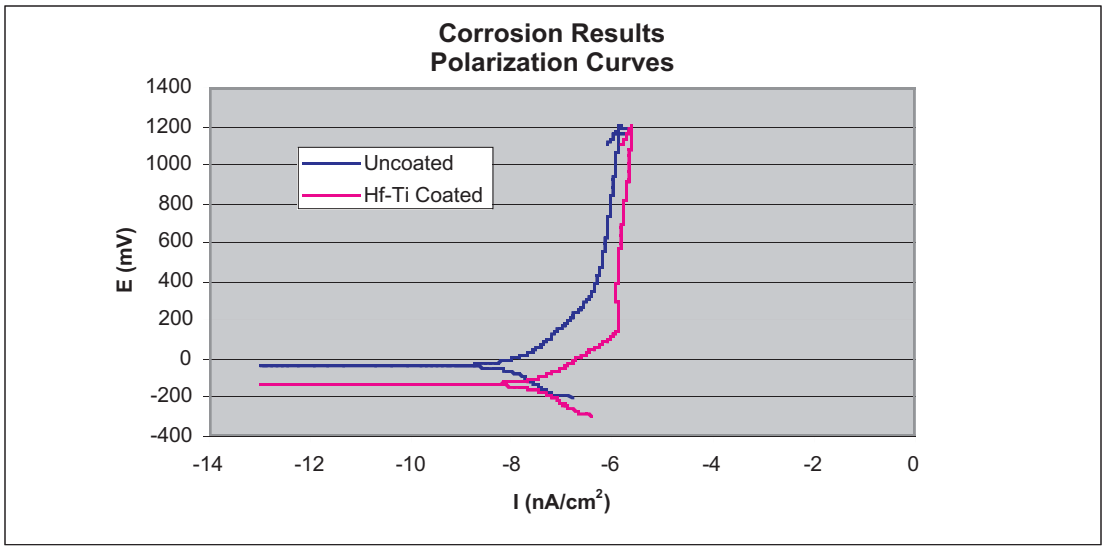

Figure 11. Corrosion test results.

IIIc. Coating of Co-Cr-Mo substrate with modified nanolaminate ceramic coating. Co-Cr-Mo used in the body as a contact surface is subject to wear. The initial rate is about 8 μm per year,[21] after which the rate decreases. A ceramic surface wears at a lower rate, but bulk ceramic is a brittle material which is subject to catastrophic failure. The approach we investigate here is the application of a ceramic coating in thin-film form, on a Co-Cr-Mo substrate. The properties of bulk materials can be modified by forming them into thin films, especially if their grain structure is nanocrystalline. This is because of the larger influence of grain boundaries, as well as the large surface-to-volume ratio of thin films.

A particular form of ceramic thin film is the nanolaminate structure,[22] formed of alternating layers of two different ceramics. The two ceramics can be, for example, ZrO_2 and Al_2O_3, which have been formed by sputtering of alternate ceramic targets in layers as thin as 3 – 3.5 nm thick. ZrO_2 is known to exist in three crystalline forms – monoclinic (low temperature to 1150°C), tetragonal (1150 – 2370°C), and cubic (above 2370°C). The addition of Al_2O_3 can stabilize the higher-temperature phases at room temperature. In addition, the existence of thin layers may improve the hardness (and toughness) of the ceramic, by confining the propagation of micro-cracks, for instance, across the boundary between layers. In this previous work, the deposited film was also subjected to heat treatment,[23] which consisted of 20 thermal cycles in air from 600° C to 1000 °C in a solar furnace. In the case of the thickest nanolaminate structure (12 nm ZrO_2/14 nm Al_2O_3), the surface hardness (measured by nanoindentation) almost doubled, increasing from 14 to 24 GPa.

To implement this idea on RHEPP-1, we switch the experiment configuration to that used for pulsed film deposition. The geometry is schematically depicted in Fig. 12. Instead of a treatment platform containing samples, the ion beam propagates to an ablation target mounted at a 45-degree angle to the beam, as shown. The target is located at 45 cm from the beam generation point, roughly the distance of maximum beam intensity on axis. In this configuration, the peak beam fluence on axis varies from about 5 to 8 J/cm^2, and the area of the target where the ablation threshold is exceeded is estimated (visually) at about 30 cm^2, depending upon the target material. The resulting ablation plume forms and travels normal to the target surface, and deposits on a substrate located typically 30 cm away from the target. There is an assembly in place in which several targets can be placed, and their positioning controlled romotely, so that targets can be alternated in-situ without breaking the vacuum. The alternating layers are thus formed by switching back and forth between the two different ceramic targets. In place of the thermal cycles mentioned above in the prior work, a portion of the coating area was subjected to 10 RHEPP-1 ion pulses in the 'surface modification' mode, at fairly low fluence (~ 1.5 J/cm^2).

To determine the thickness achievable in the ceramic layers, the deposition rate was measured for the following ceramic targets: Al_2O_3, Y_2O_3, and ZrO_2. The targets are 3 inch rounds obtained from CERAC Inc. The targets were exposed in turn to a series of 25 ion pulses from the MAP nitrogen beam. In each case, the depositional substrate was partially masked, and the mask removed after the exposure and the resulting step height measured with 1-D profilometry (DekTak). Using this procedure, the following deposition rates were measured:

Al_2O_3: 240 Å per pulse
Y_2O_3: 100 Å per pulse
ZrO_2: 184 Å per pulse

On a per-pulse basis, this is much higher than the average deposition rate per pulse using the more familiar Pulsed Laser Deposition (PLD) technique. This is because the typical laser is focused so as to concentrate the available energy, and so the equivalent area of ablation may be only a few mm^2, instead of the 30 cm^2 noted above for the pulsed beam technique.

It is assumed (but not verified) that the ratio of layer thicknesses in nanolaminates made by

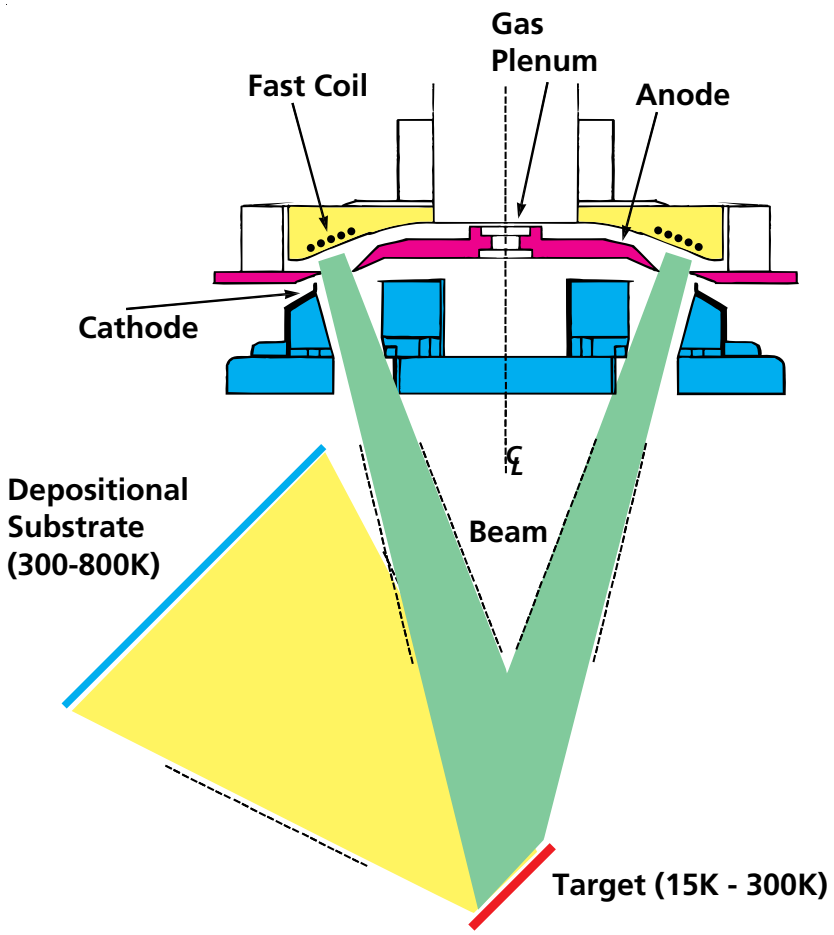

Figure 12. Schematic view of RHEPP-1 configured for thin-film formation experiments.

the alternating-target deposition technique is then proportional to the deposition rates indicated above. Therefore, the layer thicknesses for a ZrO_2-Al_2O_3 nanolaminate would in the ratio 18 nm/24 nm, and for ZrO_2-Y_2O_3 the ratio would be 18 nm/10 nm.

The first such nanolaminate coating made was with ZrO_2-Al_2O_3. Two samples were coated, one at room temperature (RT), and the other at 600°C. The number of total ion pulses was 184, and the resulting film was measured to be about 2 μm thick, although the substrate was very rough and the exact thickness was hard to determine. The RT film was pale green in appearance, and the heated sample was dark gray. No evidence of peeling or other distress was evident in the deposited coatings.

The decision was then made to switch to ZrO_2-Y_2O_3, mainly to avoid the Al component and its potential toxicity in the body. A series of 325 pulses was taken, with two Co-Cr-Mo depositional substrates, in which the target was alternated between ZrO_2 and Y_2O_3 targets after each pulse. The substrate surface was first polished with 600 grit sandpaper, then cleaned with acetone administered with a polishing pad. The substrate temperatures were RT and 200 °C. After the deposition, a portion of both substrates was subjected to the 10 low-fluence pulses as described above.

Beam treatment removed almost the entire deposited coating from the RT substrate. The treated area of the 200 °C substrate was observed to change color. Subsequent Dektak measurements showed that the treated coating remained in place,

but was roughened by the beam treatment. That heating the coating to 200°C during deposition helps it to remain in place during subsequent treatment is a rather surprising result, given that 200 °C is a modest heating level for the depositional phase. The before-treatment thickness and surface roughness (R_a) were 3 μm and 0.1 μm, respectively. After the 10-pulse treatment, the layer actually increased a little in measured thickness, and the roughness increased to 0.3 μm. The color in all cases was dark gray.

After coating and beam treatment, three surface areas were chosen for instrumented indentation testing using a Nanoindenter XP. These were: untreated Co-Co-Mo (substrate), coated but non-beam treated nanolaminate (not-treated), and coated and beam-treated nanolaminate (treated). Experiments to indentation depths of 250 nm and 1 μm were performed. The data for the 250 nm depths are discussed below, as the surface response to the deeper indent was judged to be influenced by the substrate underneath. The experiments were performed with the continuous stiffness measurement option available on the Nanoindenter XP, allowing indentation contact stiffness to measured as a function of depth. Following typical procedures, the Oliver-Pharr method was used to convert load, depth and stiffness values to hardness and modulus, the hardness values are plotted in figure 13. Ten indentation experiments were performed at selected locations on each of the three surfaces, and Fig. 13 represents the averaged results. The degree of surface roughness on each surface contributed to the scatter in the results, and 4 experiments on the not-treated surface were not included in the averaged results because measurements from those experiments indicated that they were performed at unsuitably rough locations.

It appears that the not-treated coating (blue points) is actually slightly softer than the Co-Cr-Mo substrate underneath. Treatment of the coating by the ion beam, however, substantially hardened the coating at the near surface region. The peak

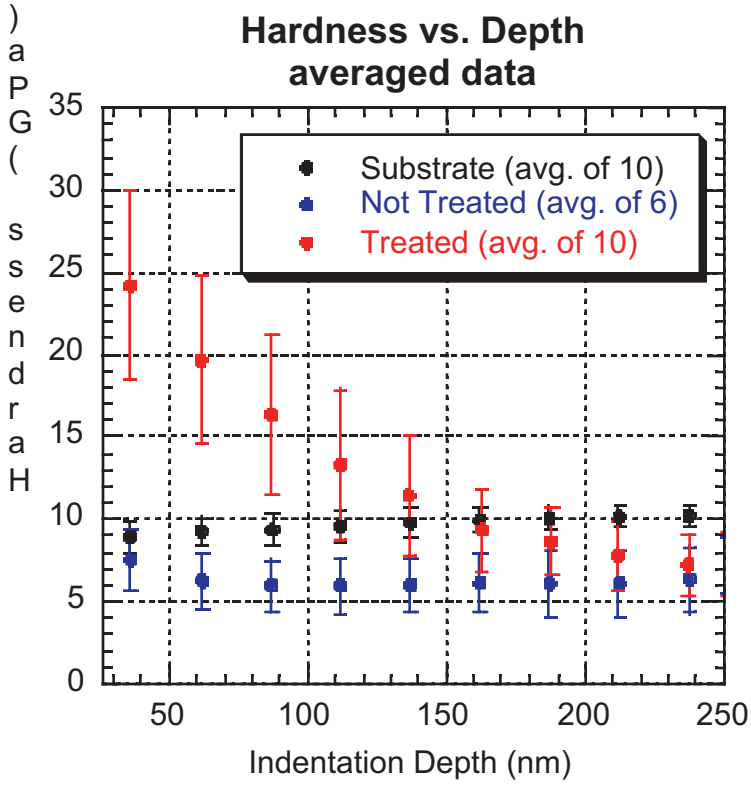

Figure 13. Surface hardness vs. nanoindentation depth

average hardness of about 25 GPa measured near the surface of the treated coating decreases linearly to about 10 GPa, the hardness of the untreated coating, at a depth of about 150 nm. This factor 2.5 increase in near-surface hardness caused by the ion treatment is similar to that seen in the earlier work with the more conventional post-deposition thermal cycling. The layer thickness obtained there (12 μm/14 μm) is similar to the estimated layer thickness here (10 μm /18 μm).

After the nanoindentation analysis, the surfaces were subjected to linear tribological pin-on-disk wear testing. Three series of 1000 cycles were performed on the substrate, as-deposited coating, and treated coating. The counterface was a Si_3N_4 1/8 inch ball operated with a load force of 10 gm, and the tests were conducted in on dry surfaces with nitrogen gas backfill.

Data from the pin-on-disk test are shown in Fig. 14. For the 1000 cycles series. The friction coefficient (y-axis), an indicator of wear and debris generation, behaves almost the same for the as-deposited and treated coating surfaces. This is different from the behavior seen in the nanoindentation study discussed above. And both coatings start out with low friction cofficient, but as the number of oscillations increases, the friction coefficient rises steadily and equals the control (Co-Cr-Mo) surface by the end of the test series.

Follow-on observations of the surface, by SEM and by FIB-XTEM, are planned, but at present the behavior difference shown by the two sets of tribological data is not understood. But the increased hardness of the treated coating, seen in the nanoindentation study, looks promising, and will be the subject of further investigation.

IV. Summary and Discussion

Three materials used in surgical body inplants have been investigated in this Report. The goal is to use intense pulsed ion beam treatment to improve the mechanical performance and biocompatibility of these materials. In the case of UHMWPE, low fluences of both electron and ion

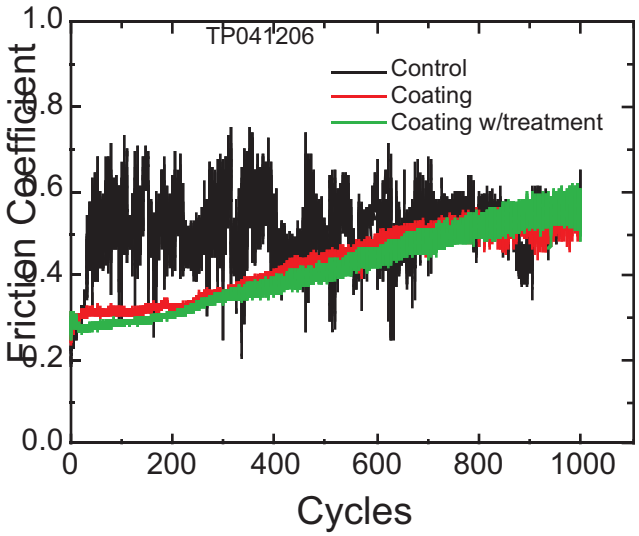

Figure 14. Pin-on-Disk data for: Co-Cr-Mo surface, and untreated and treated nanolaminate coating.

beams were applied to the surface in an attempt to induce cross-linking and produce a more wear-resistant surface. Several different treatment protocols were used on the flat Marathon samples provided by DePuy, and all but the lowest ion beam fluence resulted in significant degradation of the Marathon bulk properties. In the case of the lowest Ion beam fluence (0.1 to 0.2 J/cm^2 Ne beam, 10 pulses), no significant bulk property degradation was seen, and follow-on Pin-on-Disk testing of Marathon treated at this level is planned.

A surface-alloyed layer of Hf/Ti that has been previously been shown to exhibit improved wear durability was subjected to biocompatibility and corrosion testing. These tests showed that the treated surface produced a favorable cell growth response when live Saos-2 cells were introduced in a liquid medium in contact with this surface. The gain in cell response was 60% higher than the Control (plastic) case after a 7 day incubation period. This may be caused either by the introduction of Hf to the near-surface zone, the suppression of the toxic elements Al and V from the near-surface zone, or both. No significant change in the corrosion resistance was seen compared to the

base Ti-6Al-4V substrate material.

We have experimented with the formation of a nanolaminate thin-film coating over a Co-Cr-Mo substrate, made by repeatedly ablating two ceramic targets, Y_2O_3 and ZrO_2, first one and then the other. The resultant 3 μm layer was then treated by the same ion beam at reduced fluence for 10 pulses. Nanoindentation of the coated/untreated and coated/treated layer showed a significant hardening of the treated layer (25 GPa), compared to either the coated/untreated layer (8 GPa) or the base Co-Cr-Mo (10 GpA). Subsequent Pin-on-Disk tests indicated that either coating performed initially with lower friction coefficient, compared to the base Co-Cr-Mo. But as the number of cycles was increased towards 1000, the coefficient increased steadily and reached the level of the Co-Cr-Mo by the end of the series. Further microstructural analysis (SEM and FIB/XTEM) is needed to determine to cause of the behavior seen in these two mechanical tests.

Further investigation is planned in all the cases mentioned above. In addition, there has been much interest recently in coatings formed of diamond-like-carbon, or amorphous carbon coatings in general. Researchers have noted both improvements in mechanical wear performance, and a reduction in surface friction. Some investigation of this type of coating using ion beam ablation may be worthwhile, since such coatings have already been produced, and exhibit promising properties. However, heat treatment by ion beam, as used above with the ceramic nanolaminate coatings, is not expected to produce favorable results. This is because such carbon coatings undergo a transition to the graphitic Sp3 phase when the coating temperature reaches 600°C, a temperature which is easily reached by the ion beam treatment.

V. Acknowledgement

Gerard Torres provided able technical assistance for the RHEPP-1 experiments.

This work was supported by the United States Department of Energy under Contract DE-AC04-94AL85000. Sandia is a multi-program laboratory operated by Sandia Corporation, a Lockheed Martin Company, for the United States Department of Energy.

VI. References

[1]P. Soderman, H. Malchau, P. Herberts, R. Zugner, H. Regner, G. Garellick, Outcome After Total Hip Arthroplasty: Part II. Disease-Specific Follow-up and the Swedish National Total Hip Arthroplasty Register. Acta Orthop Scand. **72(2)**, 113-9 (2001).

[2]C. A. Engh Jr., A. M. Claus, R. H. Hopper Jr., C. A. Engh, Long-Term Results Using the Anatomic Medullary Locking Hip Prosthesis, Clin Orthop. **393**, 137-46 (2001).

[3]J.Older, Charnley Low-Friction Arthroplasty: A Worldwide Retrospective Review at 15 to 20 years, J Arthroplasty **17(6)**, 675-80 (2002).

[4]E. Garcia-Cimbrelo, A. Cruz-Pardos, J. Cordero, J. Sanchez-Sotelo, Low-Friction Arthroplasty in Patients Younger than 40 Years Old: 20- to 25-Year Results, J Arthroplasty **15(7)**, 825-32 (2000).

[5]C. A. Engh, R. H. Hopper Jr., Porous-Coated Total Hip Arthroplasty in the Young, Orthopedics **21(9)**, 953-6 (1998).

[6]D. H. Sochart, Relationship of Acetabular Wear to Osteolysis and Loosening in Total Hip Arthroplasty, Clin Orthop. **363**, 135-50 (1999).

[7]C. A. Engh, Jr., R. H. Hopper Jr., C. A. Engh, J. P. McAuley, Wear-Through of a Modular Polyethylene Liner: Four Case Reports. Clin Orthop. **383**, 175-82 (2001).

[8]Timothy J. Renk, Paula P. Provencio, Somuri V. Prasad, Anatoli S. Shlapakovski, Anatoly V. Petrov, Kiyoshi Yatsui, Weihua Jiang, and Hisayuki Suematsu, Materials Modification using Ion Beams, Proc. of the IEEE **92**, 1057-1081 (2004).

[9]H. C. Harjes, K. J. Penn, K. W. Reed, C. R.

McClenahan, G. E. Laderach, R. W. Wavrik, J. L. Adcock, M. E. Butler, G. A. Mann, G. E. Pena, G. J. Weber, D. VanDeValde, L. E. Martinez, D. Muirhead, P. D. Kiekel, D. L. Johnson, and E. L. Neau, Initial Results from the RHEPP module, in D. Mosher and G. Cooperstein (eds.), 9th International Conference on High-Power Particle Beams (Beams 92), Washington, DC, NTIS PB92-206168, pp. 333-340.

[10]T. J. Renk, R. G. Buchheit, N. R. Sorensen, D. C. Senft, M. O. Thompson, and K. S. Grabowski, Improvement of surface properties by modification and alloying with high-power ion beams, Phys. Plasmas **5**, 2144-2150 (1998).

[11]J. P. Biersack. J. F. Ziegler, Transport of Ions in Matter, IBM Research, Yorktown Heights, NY, 1995.

[12]G. Mueller, G. Schumacher, D. Strauss et al, in Proceedings of the 11th International Conference on High Power Particle Beams (BEAMS' 96), Prague, K. Jungwirth and J. Ullschmied, Eds., Vol. 1, 1996, pp. 267-271.

[13]V. Engelko, B. Yatsenko, G. Mueller, H. Bluhm, Vacuum **62**, 211-215 (2001).

[14]G. Digas, J. Kärrholm, B. Nivbrant, S. Röhrl, J. Thanner, Increased Femoral Head Penetration Using Polyethylene Sterilized with Ethylene Oxide, Presented at the European Federation of National Associations of Orthopaedics and Traumatology, Rhodes Congress, Greece; June 1-7 (2001).

[15]L. S. Bargmann, B. C. Bargmann, J. P. Collier, B. H. Currier, M. B. Mayor, Current Sterilization and Packaging Methods for Polyethylene, Clin Orthop. **369**, 49-58 (1999).

[16]J. P. Collier, L. C. Sutula, B. H. Currier, J. H. Currier, R. E. Wooding, I. R. Williams, K. B. Farber, M. B. Mayor, Overview of polyethylene as a Bearing Material: Comparison of Sterilization Methods, Clin Orthop. **333**, 76-86 (1996).

[17]B. H. Currier, J. H. Currier, J. P. Collier, M. B. Mayor, R. D. Scott, Shelf Life and In Vivo Duration: Impacts on Performance of Tibial Bearings. Clin Orthop. **342**, 111-2 (1997).

[18]T. J. Renk, P. P. Provencio, P. G. Clem, S. V. Prasad, and M. O. Thompson, Use of Intense Ion Beams for Surface Modification and Creation of New Materials, SAND Report **SAND2002-4215** (Unlimited Release), December 2002.

[19]H. Matsuno, A. Yokoyama, F. Watari, M. Uo, and T. Kawasaki, Biocompatibility and osteogenesis of refractory metal implants, titanium, hafnium, niobium, tantalum and rhenium, Biomaterials **22**, 1253-1262 (2001).

[20]U. Landegren, Measurement of Cell Numbers by Means of the Endogenous Enzyme Hexosaminidase. Applications to Detection of Lymphokines and Cell Surface Antigents, Journal of Immunological Methods **67**, 379-388 (1984).

[21]Robert Hopper, AORI, Alexandria, VA, private conversation.

[22]V. Teixeira, A. Monteiro, J. Duarte, and A. Portinha, Deposition of composite and nanolaminate coatings by sputtering, Vacuum **67**, 477-483 (2002).

[23]J. O. Carneiro, V. Teixeira, A. Portinha, S. N. Dub, and R. Shmegera, Hardness Evaluation of Nanolayered PVD Coatings using Nanoindentation, Rev. Adv. Mater. Sci. **7**, 83-90 (2004).

DISTRIBUTION

Unclassified Unlimited Release

1	MS9018	Central Technical Files, 8945-1
2	MS0899	Technical Library, 9616

10 Dr. Vladimir Engelko
D.V. Efremov Scientific Research Institute of the
Electrophysical Apparatus
Metallostroy
St. Petersburg 196641
Russia

10 Donald P. McNulty
DePuy Orthopaedics, Inc.
P. O. Box 988
700 Orthopaedic Drive
Warsaw, IN 46581-0988

20 Dr. Thomas D. Petersen
Alavarado Orthopedic Research
9680 Alto Dr.
La Mesa, CA 91941

Internal Distribution

1	MS0123	LDRD, Donna Chavez, 1011
10	MS1421	Paula P. Provencio, 1111
1	MS1056	Barney L. Doyle, 1111
10	MS0889	Somuri V. Prasad, 1851
10	MS0889	Thomas E. Buchheit, 1851
1	MS0889	Jonathan S. Custer, 1851
20	MS1182	Timothy J. Renk, 15335
10	MS1182	Bob N. Turman, 15335
1	MS1153	Malcolm T. Buttram, 15330
1	MS1165	Richard J. Steichen, 15300
1	MS1221	James A. Tegnelia, 15000
1	MS1193	John E. Maenchen, 1645
1	MS1190	C. L. Olson, 1600
1	MS1190	M. Keith Matzen, 1600
1	MS0888	Roger Clough, 1811
1	MS1411	Mathias C. Celina, 1811
1	MS1427	Julia M. Phillips, 1100
1	MS0839	Gerold Yonas, 16000
1	MS0839	Curtis Johnson, 16001